Targeting the Weak Spot: Preferential Disruption of Bacterial Poles by Janus Nanoparticles

Danh Nguyen,[1,†] Swagata Bhattacharyya,[2,†] Hunter Richman,[2] Yan Yu,[2,] Ying Li,[1,*]*

[1] Department of Mechanical Engineering, University of Wisconsin-Madison, Madison, WI, 53706, United States

[2] Department of Chemistry, Indiana University, Bloomington, IN, 47405, United States

ABSTRACT: The interaction between nanoparticles (NPs) and bacterial cell envelopes is crucial for designing effective antibacterial materials against multi-drug-resistant pathogens. However, current understanding assumes a uniform bacterial cell wall. This study challenges that assumption by investigating how bacterial cell wall curvature impacts antibacterial NP action. Focusing on Janus NPs, which feature segregated hydrophobic and polycationic ligands and previously demonstrated high efficacy against diverse bacteria, we find that these NPs preferentially target and disrupt bacterial poles. Experimental and computational approaches reveal that curvature at *E. coli* poles induces conformational changes in lipopolysaccharide (LPS) polymers on the outer membrane, exposing underlying lipids for NP-mediated disruption. We establish that curvature-induced targeting by Janus NPs depends on outer membrane composition and is most pronounced at physiologically relevant LPS densities. This work demonstrates that high-curvature regions of

bacterial cell walls are “weak spots” for Janus NPs, thereby aiding the development of more effective targeted therapies.

KEYWORDS: Janus nanoparticles, bacterial membrane, antibacterial nanomaterials, bacterial cell curvature, lipopolysaccharide conformation, membrane disruption

The rise of antibiotic-resistant bacteria is a significant global health threat.[1] To address this, antibacterial nanoparticles (NPs) are being developed as an alternative to traditional antibiotics. These NPs often employ multiple mechanisms, making them less susceptible to resistance development.[2-6] A dominant mechanism is targeting the bacterial cell envelope, essential for maintaining cell shape and viability.[7-9] Interactions of NPs with the bacterial cell wall have been studied extensively.[10-12] Experimentally, most studies focus on the overall antibacterial effects, including cell viability and whole-population measurements of NP-induced cell wall penetration.[13-15] Some studies have quantified NP binding kinetics to bacterial cell surface.[16-22] Computational simulations of NP-membrane interactions have also been done extensively to elucidate underlying mechanisms.[23-31] All these studies were based on the assumption that bacteria have uniform cell walls. However, recent studies challenge this assumption.

Recent works, largely enabled by the advancement of high-resolution imaging techniques, have revealed that the outer membrane of a diverse range of Gram-positive and Gram-negative bacteria is highly spatially heterogeneous. Different regions along the bacterial cell wall vary significantly in composition, curvature, and function.[32, 33] Mounting evidence suggests that cell wall curvature plays an important role in driving the heterogeneous distribution of lipids and proteins on bacterial surface.[34] For instance, studies have reported the accumulation of certain negatively charged molecules, including the phospholipid cardiolipin, on the cell poles of rod-shaped bacteria due to

their preference for high curvature. Several cell division proteins have also been shown to localize at high-curvature sites including the cell poles and cell division site.[34-40] Computational studies have corroborated these findings, revealing different mechanisms by which membrane curvature can affect local distribution of lipids, such as curvature-induced membrane thinning or lipid sorting.[41-53] Despite those pioneering findings, no studies have addressed the question: how might the curvature of the bacterial cell wall affect their interaction with antibacterial NPs?

Bacterial cell walls are covered with highly charged, bulky lipoglycans, such as peptidoglycan on Gram-positive bacteria and lipopolysaccharide (LPS) on Gram-negative bacteria. Taking LPS as an example, their chemical structure and surface density govern the interaction with NPs and some antibiotics.[54-57] However, we propose that, like other grafted polymers,[58-70] the conformation of LPS depends on the curvature of the bacterial cell wall. For instance, grafted poly(ethylene glycol) forms a "mushroom" conformation on curved surfaces and a "brush" on flatter surfaces.[62] This curvature-dependent polymer conformation directly determines the physical adsorption of proteins on NP surfaces.[59] Thus, we hypothesize that bacterial cell wall curvature affects the LPS packing conformation and, consequently, NP-membrane interaction.

This study tests our hypothesis by examining interactions between Janus NPs and *E. coli*. These "two-faced" NPs display hydrophobic and polycationic ligands separately on two hemispheres. We previously demonstrated that amphiphilic Janus NPs are more effective in disrupting lipid membranes[71-73] and killing bacteria than uniformly coated NPs.[74] Here, we demonstrate that the Janus NPs preferentially bind to and disrupt *E. coli* poles. Through experiments and computational simulations, we show how curvature of the bacterial pole versus along the axial wall influences LPS conformation, making the Janus NPs more effective in penetrating the LPS layer and disrupting the outer membrane. Our molecular dynamics simulation establishes a diagram

predicting the dependence of Janus NP-outer membrane interactions on bacterial cell wall curvature within a broad range of outer membrane compositions. Our results suggest that bacterial cell wall heterogeneity could reveal targets for effective antibacterial strategies.

The Janus NPs used in this study have a hydrophobic hemisphere and a polycationic hemisphere (Figure 1a). We achieved this Janus structure by coating one hemisphere of aminated silica NPs with 5-nm thick chromium and 25-nm thick gold layers, then conjugating octadecanethiol onto the gold cap to make it hydrophobic. Colistin was then conjugated onto the aminated hemisphere using glutaraldehyde crosslinking chemistry (col/pho JP). While colistin is often used as a last-resort antibiotic, we employed it here as a polycationic ligand to promote strong electrostatic interaction of Janus NPs with bacterial membranes, as we reported previously.[74] The Janus geometry and hydrodynamic diameter of these NPs was confirmed, respectively, using scanning electron microscopy (SEM) (Figure 1b) and Dynamic Light Scattering (Figure S1).

To evaluate the impact of the Janus NPs on bacterial membranes, we incubated *E. coli* (MG1655 strain) with various NP concentrations for 2 h at 37°C with shaking. SEM micrographs revealed that Janus NPs preferentially interacted with the *E. coli* poles (Figures 1c,d). Notably, a significant majority of *E. coli* in contact with the Janus NPs exhibited deformed or even ruptured cell envelopes at the poles (Figures 1c,d). Although some of the Janus NPs exhibited slight aggregation, this did not affect their preferential binding. Control experiments using uniform cationic NPs (col UPs) without hydrophobic ligands (zeta potential in Figure S2) showed attachment to both the poles and axial cell wall of *E. coli* with no preference (Figures 1e,f). We have shown previously that once Janus NPs are brought into close proximity with lipid membranes after electrostatic attraction, their surface hydrophobicity on one hemisphere drives the lipid extraction, leading to membrane disruption.[71-73] The difference in binding between Janus NPs and

uniform colistin NPs here suggests that in the presence of electrostatic attraction between the cationic charges on NPs and anionic bacterial membranes, the hydrophobic interaction with the lipids underneath the LPS layer plays an important role in the preferential binding of Janus NPs to the bacterial pole. This is confirmed by roughly identifying the orientation of the Janus NPs in the SEM micrographs (Figure 1g) and found that over half were oriented with their hydrophobic hemisphere facing the bacterial membrane (Figure 1h). In the SEM images, the hydrophobic hemisphere appeared brighter due to strong electron scattering of the gold coating.

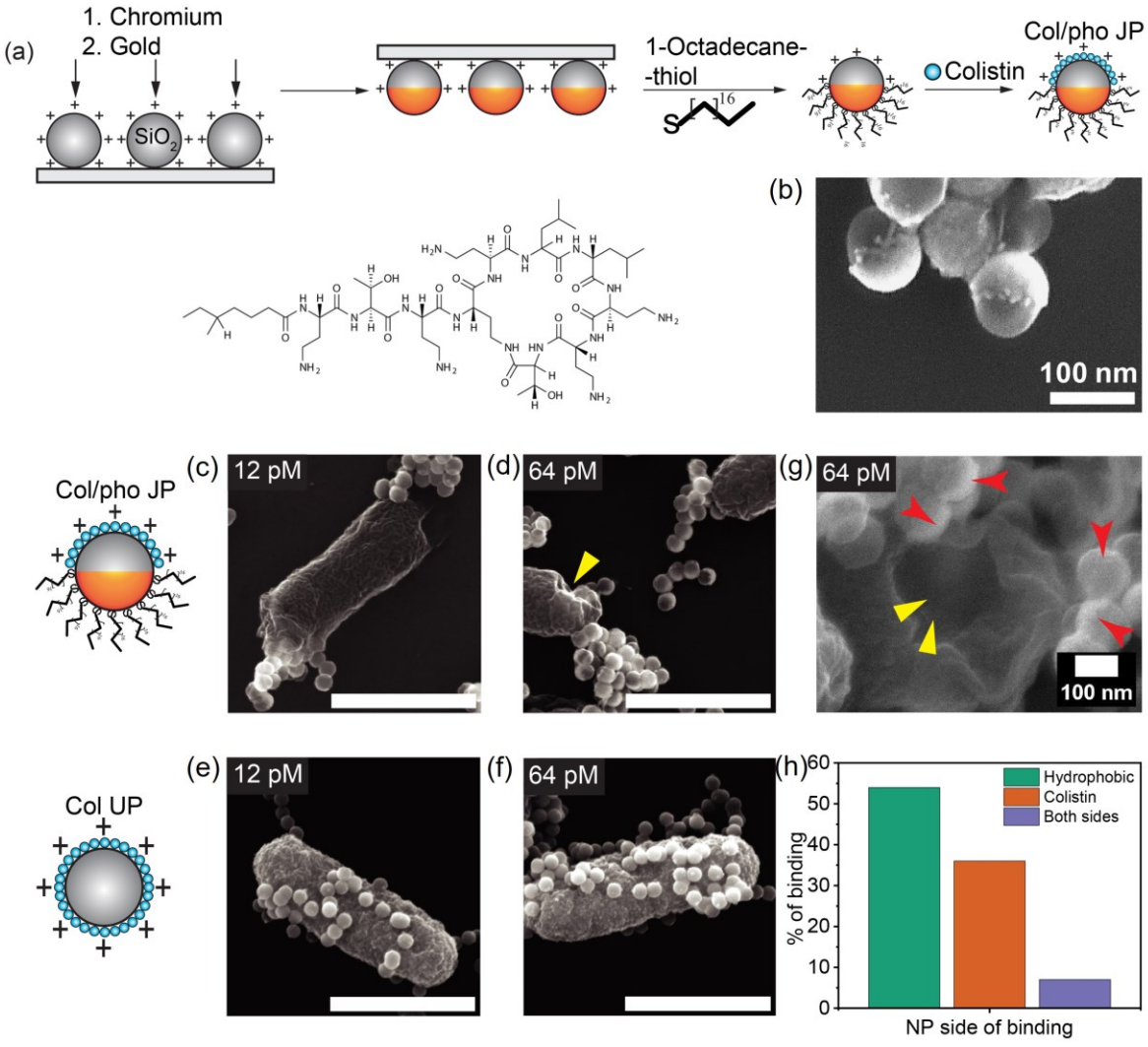

Figure 1. (a) Schematic illustration of the fabrication of Janus NP. (b) SEM image of the Janus NPs. (c,d) SEM images showing *E. coli* interaction with Janus NPs at 12 pM and 64 pM

concentrations. Scale bars, 1 μm. Yellow arrows indicate deformations and ruptures in the bacterial cell wall. (e, f) SEM images showing *E. coli* interaction with uniform cationic NPs (col UP) at 12 pM and 64 pM concentrations. Scale bars, 1 μm. (g) SEM images showing Janus NPs (64 pM) interacting with *E. coli* with different sites of binding. Yellow arrows indicate deformations and ruptures in the bacterial cell wall. Red arrows indicate the hydrophobic side of Janus NPs. (h) Data from SEM image analysis show the percentage of Janus NPs bound to the bacterial surface from their hydrophobic side, cationic colistin-coated side, or the Janus interface (both sides).

We next directly visualized the interaction of Janus NPs with bacteria using live-cell imaging. The colistin-coated hemisphere of the Janus NPs was conjugated with a trace amount of Cy5 HNS ester dye without altering their surface chemistry, so the NPs were fluorescent for visualization (Figure S3). During live-cell imaging, Janus NP concentration was maintained at 12 pM for optimal visualization. By combining fluorescence imaging of the NPs with bright-field imaging of the bacteria, we observed preferential attachment of Janus NPs to the bacterial poles (Figures 2a-c). This interaction was strong enough to maintain NP attachment even when bacteria "tumbled" in solution (Video S1). Approximately 68% of NPs are attached to the bacterial pole, while only about 18% are attached to the axial wall of the rod-shaped bacteria (Figure 2c).

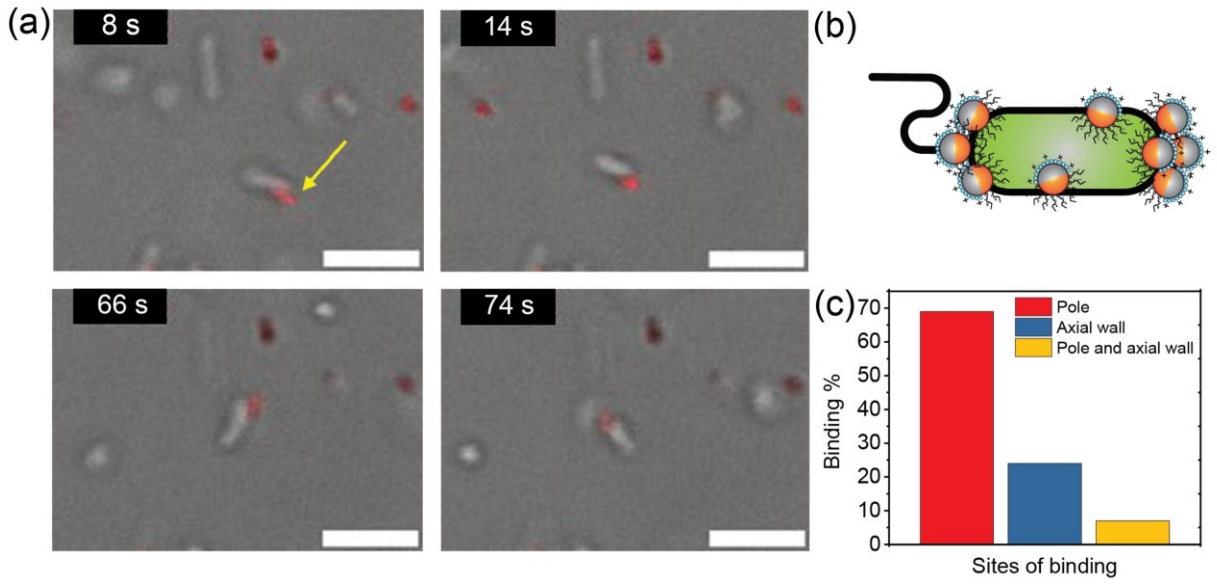

Figure 2. (a) Overlaid fluorescence and bright-field time-lapse images showing the interaction of fluorescently labeled Janus NPs (shown in red) with *E. coli*. Scale bars, 4 μm. (b, c) Analysis from live cell images shows the percentage of *E. coli* bacteria with Janus NPs bound to the poles, axial wall, or both regions.

We next investigated whether our observations were broadly applicable to Janus NPs of different sizes and coated with other polycationic ligands. To assess the effect of NP size, we prepared 50 nm hydrophobic/cationic Janus NPs using the same procedures. Live cell imaging and SEM revealed that these smaller Janus NPs, like the 100 nm ones, preferentially interacted with and disrupted the poles of *E. coli* (Figure S4). To examine the effect of polycationic ligands, we replaced colistin with a generation 1.0 PAMAM dendrimer, which has eight primary amines (comparable to colistin's seven) but is not antibiotic. The resulting dendrimer-coated Janus NPs, referred to as dend/pho Janus NPs, were characterized for their hydrodynamic diameter and zeta potential (Figures S5 and S6). We found that dend/pho Janus NPs also preferentially bound to the poles of *E. coli* (Figure S7). Collectively, these results confirm that the preferential interaction of

Janus NPs with bacterial poles is a general phenomenon driven primarily by the high curvature of the cell wall, rather than the specific type of ligand or NP size.

Why do Janus NPs preferentially bind and disrupt bacterial poles? While many factors, such as protein or lipid accumulation on the poles,[34, 39, 75, 76] may play a role, here we focused on curvature. We previously demonstrated that polycationic ligands on Janus NPs enhance their electrostatic attraction to lipopolysaccharide (LPS) on the outer membrane of Gram-negative bacteria.[74] Following this binding, the NP's hydrophobic hemisphere disrupts the membrane by extracting lipids and compressing it.[71-73] Since surface curvature influences the conformation of grafted polymers,[64, 77-79] we propose that the distinct curvatures of bacterial poles and axial walls affect LPS configuration, influencing Janus NP interactions with the bacterial membrane.

To understand the observed phenomenon, we performed coarse-grained (CG) molecular dynamics (MD) simulations. We modeled bacterial membranes with different curvatures: flat membranes for axial cell walls and vesicles for high-curvature poles (Figure 3a). Tests with vesicle sizes from 27 to 54 nm showed similar interactions with Janus NPs (Figure S10). Using Martini force field CG models of LPS,[80] which capture key LPS features without the O-antigen, we modeled rough (RaLPS) and truncated (ReLPS) LPS, with RaLPS being bulkier due to more sugar core beads (Figures 3a, S8). The membrane also included POPE lipids, a common bacterial membrane lipid,[81] with an RaLPS ratio of 60:40, reflecting typical bacterial LPS coverage. At this membrane composition, RaLPS covers about 75% of the curved membrane surface and 87% of the flat membrane surface, representing the typical LPS surface coverage on the bacterial surface as previously reported.[82-84] These CG models better capture the complexity of the bacterial outer membrane than other more simplified models.[85-90]

To quantify the curvature effect on LPS packing, we analyzed RaLPS surface coverage (%) (Figure 3b-i), core bead density (Figure 3b-ii), and the center-of-mass (COM) distance between RaLPS molecules (Figure 3b-iii). Results showed significantly denser LPS packing on flat versus curved membranes, with higher LPS content yielding denser packing in both cases.

To further characterize RaLPS conformation, we quantified two parameters: the radius of gyration (R_g) of RaLPS core beads (Figure 3b-iv) and the average COM distance between RaLPS core beads and POPE head groups (PO_4^-) ($D_{Pe\text{-}S}$, nm) (Figure 3b-v). R_g of RaLPS is significantly larger on flat membranes, especially with higher RaLPS content. This indicates a more extended conformation, consistent with what is known for polymer brushes.[91] This was further supported by larger $D_{Pe\text{-}S}$ values on flat membrane, which increase with RaLPS content. This shows that DOPE lipids are closer to the LPS layer on curved regions. These results suggest that curvature affects both LPS packing and conformation; on curved membranes, LPS adopts a "mushroom" rather than "brush" configuration, exposing more POPE lipids.

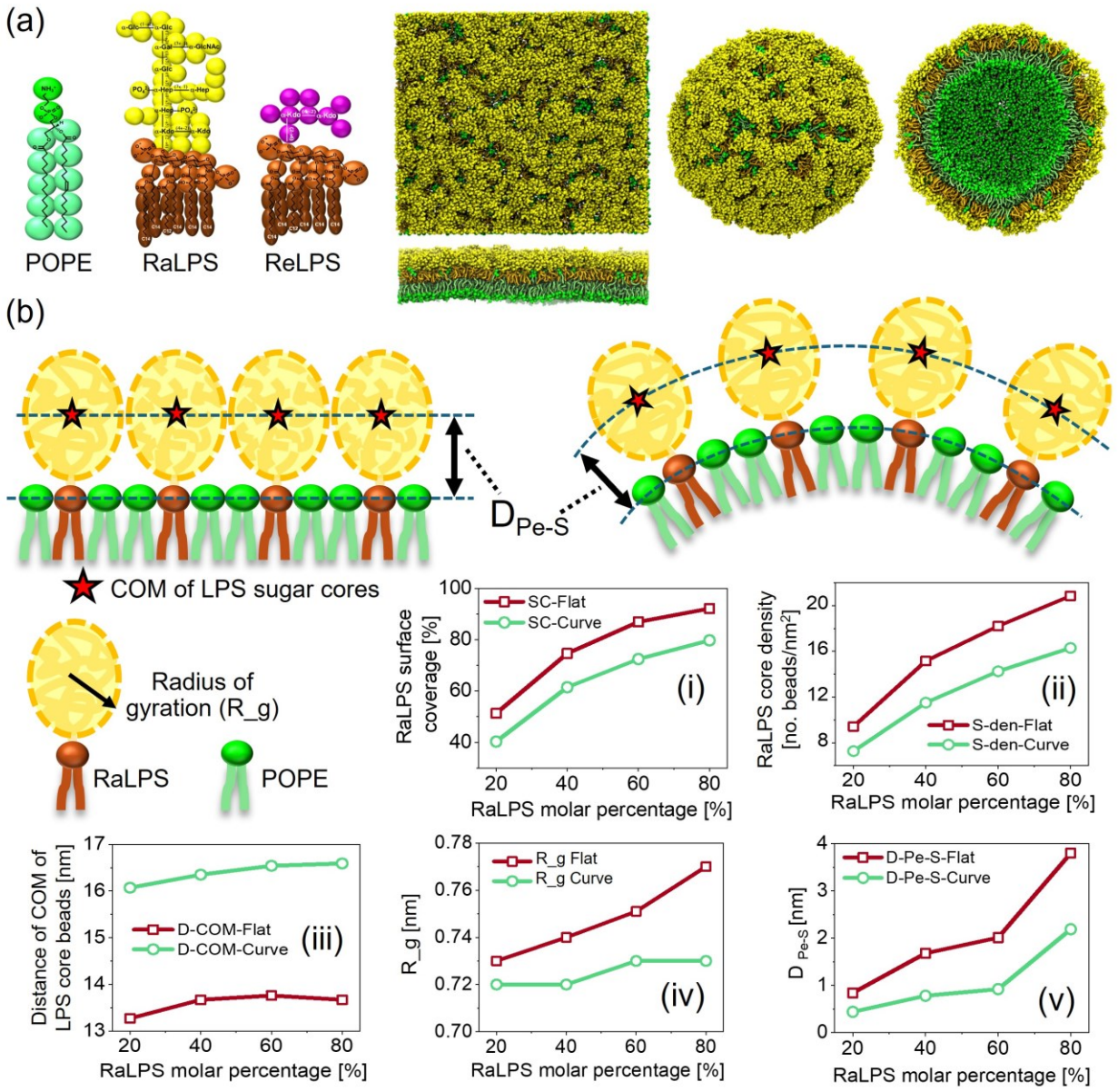

Figure 3. Molecular model of the bacterial membrane and the influence of membrane curvature on the packing of LPS. (a) The bacterial cell membrane has three major components: POPE, RaLPS, and ReLPS. CG representation illustrates the distribution of RaLPS and POPE in two membrane geometries: planar membrane (representing low-curvature membranes) and vesicle (representing highly curved membranes). An example of a 60% RaLPS: 40% POPE membrane configuration after 5 μs of relaxation is shown. POPE beads and tails: green and lime, respectively.

RaLPS core beads and tails: yellow and brown, respectively. ReLPS core beads and tails: purple and brown, respectively. The flat membrane dimension is ~ 30 × 30 nm². The vesicle diameter is ~27 nm. (b) Influence of curvature on the distribution of RaLPS on the membrane surface. This analysis focuses on RaLPS core beads, including (i) surface coverage percentage, (ii) core bead density (number of beads/nm^2), (iii) center of mass (COM) distance between RaLPS core beads, (iv) radius of gyration of RaLPS core beads (R_g, nm), and (v) the average distance between RaLPS core beads and POPE head beads ($D_{Pe\text{-}S}$, nm). For clarity, solvent molecules are included in the simulation but are not shown here.

How do the different LPS packing and conformation affect Janus NP interactions with bacterial membranes? We analyzed the binding energy of Janus NPs on both flat and curved membranes. Using our prior Janus NP model,[74] with a 10 nm gold core and hydrophobic/hydrophilic hemispheres (Figure 4a), the Janus NP measures approximately 15 nm in diameter. We used umbrella sampling simulations to measure free energy as a function of the COM distance between the Janus NP and membrane (Figure 4b). The NP was positioned to maximize hydrophobic and electrostatic interactions, as this configuration best disrupts membranes.[74, 92] Indeed, alternative configurations – facing the membrane with only the colistin or hydrophobic hemisphere – failed to disrupt the membrane after 2000 ns of simulation (Figure S11). We further analyzed the radial distribution function (RDF) of POPE and RaLPS components (Figure 4c) to identify likely NP contact points during binding (Figures 4e,g).

On the flat membrane, the system's energy decreases as the NP approaches the membrane, reaching a minimum at point (2) due to an initial electrostatic attraction with RaLPS (Figure 4d). Figure 4e shows that the NP likely attracts the negatively charged groups and core beads of RaLPS. However, as the NP penetrates deeper (2 → 3), steric repulsion increases due to the higher density

of LPS core beads. This repulsion eventually outweighs the electrostatic attraction and leads to a significant increase in free energy.

Similarly, on the curved membrane, free energy decreases as the NP approaches (point 2*), but further penetration (2* → 3*) experiences weaker repulsion (Figure 4f). The RDF reveals an approximately 2.5-fold decrease in RaLPS core bead density at point 3* (curved) compared to point 3 (flat) (Figure 4e). Additionally, a higher density of POPE lipids near the particle at point 3* (curved) suggests potential hydrophobic attractions between the NP and these lipids, unlike the negligible interaction observed in the flat membrane (point 3).

These findings highlight two key points regarding the interactions between Janus NPs and bacterial membranes. First, the brush-like conformation of RaLPS on flat membranes limits the deep penetration of Janus NPs. In contrast, curved membranes, which feature less densely packed RaLPS and readily exposed POPE lipids, allow for stronger NP attachment. Overall, both electrostatic and hydrophobic interactions are critical in driving Janus NP interactions with bacterial membranes. Electrostatic attractions initially bring the Janus NPs close to the LPS membranes, but the extent of steric repulsion varies depending on LPS conformation, which is influenced by membrane curvature. Only in regions of high curvature, where RaLPS is less densely packed and steric repulsion is reduced, can Janus NPs effectively attach to and disrupt the lipid membrane beneath the LPS layer through hydrophobic interactions.

.

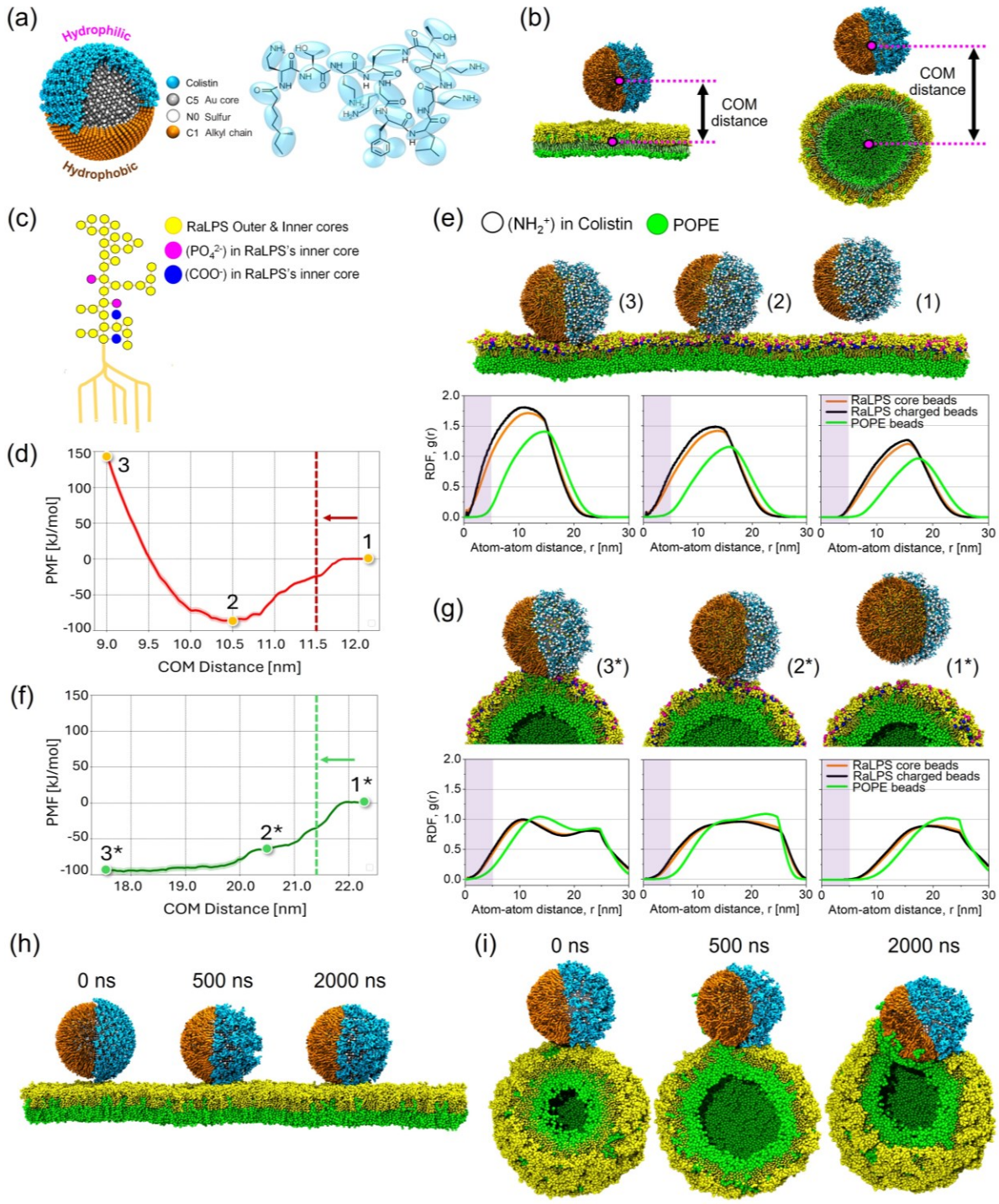

Figure 4. Molecular mechanisms for Janus NP binding to flat and curved bacterial membranes. (a) CG representation of the Janus NP with a core diameter of 10 nm. (b) Initial setup for umbrella sampling simulations to study the Janus NP binding to bacterial membranes. The flat membrane

dimension is ~ 30 × 30 nm². The vesicle diameter is ~27 nm. The membranes consist of 60% RaLPS and 40% POPE molar concentration. (c) Components within a RaLPS molecule are used for radial distribution function (RDF) calculations. (d) Potential of mean force (PMF) illustrating Janus NP-flat membrane interaction. The dashed line indicates the COM distance when the NP touches the membrane. (e) Snapshots and RDF from key states along the PMF profiles of Janus NP-flat membrane interaction. The shaded area in RDF plots indicates close contact between NP and membrane (distance < 5.0 nm). (f) PMF demonstrating Janus NP-curved membrane interaction. The dashed line indicates the COM distance when the NP touches the membrane. (g) Snapshots and RDF from key states along the PMF profiles of Janus NP-curved membrane interaction. The shaded area in RDF plots indicates close contact between NP and membrane (distance < 5.0 nm). MD snapshots of the interaction of Janus NP with (h) a planar membrane and with (i) a curved membrane over 2000 ns. RaLPS: yellow beads. POPE: green beads. For clarity, solvent molecules are included in the simulation but are not shown here.

After establishing the effect of membrane curvature on Janus NP binding, we investigated the membrane disruption process. Consistent with our bacterial experiments, where conjugated NPs induced deformations or ruptures at the poles (Figures 1d-f), simulations revealed that Janus NPs primarily disrupt the curved membranes of bacterial models. We conducted 2000 ns free dynamics simulations, verified across three duplicate runs (Figures S14, S15). As expected, the Janus NP did not cause significant deformation on flat membranes (Figure 4h). This aligns with the binding energy calculations that indicate substantial steric hindrance from densely packed LPS "brushes" (Figures 4d,e). In contrast, the Janus NP easily penetrated the curved membrane, extracting POPE lipids (green beads) with its hydrophobic ligands and ultimately disrupting the membrane (Figure

4i). This observation aligns with the binding energy calculations in Figures 4f,g, which show that curvature enhances NP attachment and access to POPE lipids.

MD simulation also confirms that a uniform cationic NP does not disrupt the curved membrane (Figure S16), matching our experimental observations (Figures 1e,f). To further assess the role of membrane curvature, we simulated a cylindrical membrane to mimic the axial cell wall and observed that the Janus NP only attached to the surface without penetrating or disrupting the membrane (Figure S17), similar to the results with flat membranes (Figures 4h, S14).

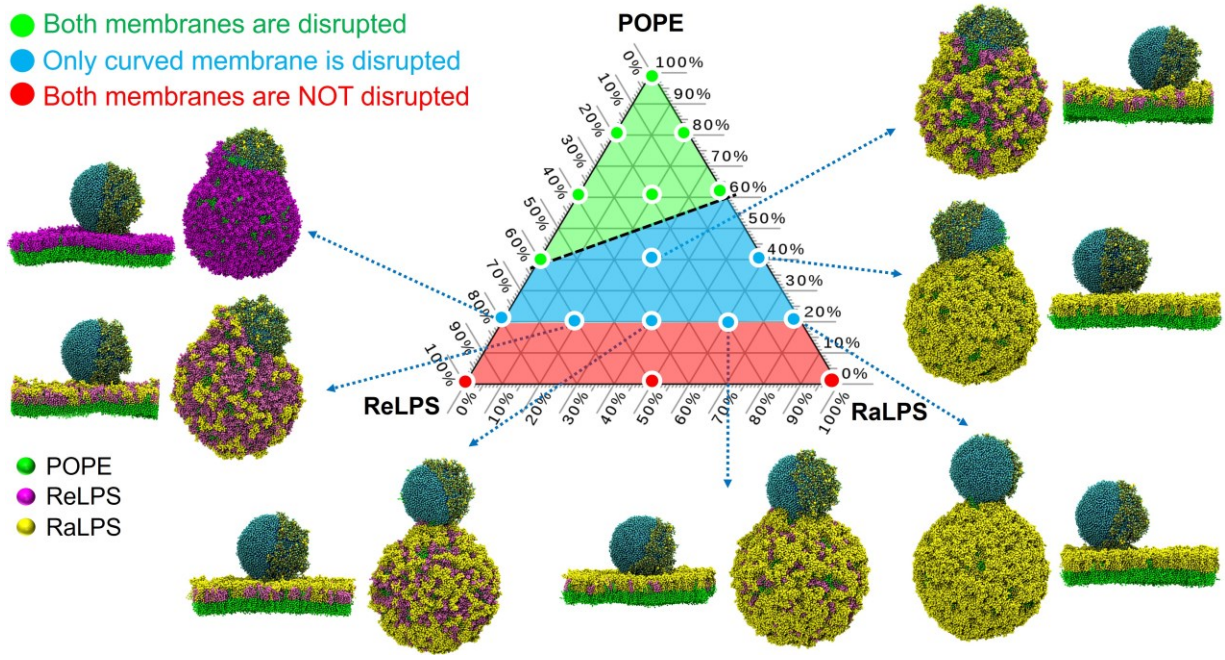

Figure 5. Tertiary diagram illustrating Janus NP interaction with bacterial membranes on planar and curved surfaces. The disruption efficacy of Janus NPs across 17 different POPE/RaLPS/ReLPS compositions are represented as points in the phase diagram. The flat membrane dimension is ~ 30 × 30 nm². The vesicle diameter is ~27 nm. RaLPS: yellow beads. ReLPS: purple beads. POPE: green beads. For clarity, solvent molecules are included in the simulation but are not shown.

Bacteria have diverse outer membrane compositions and some can even modify their LPS content[93, 94] and cell wall organization [95-97] in response to antibiotics. We investigated how the preferential interaction of Janus NPs with bacterial poles depends on outer membrane composition, particularly the surface concentration of LPS. In our model, membranes composed of RaLPS, ReLPS, and POPE for both flat and curved geometries. We allowed the Janus NP to interact with a broad range of these compositions (Figure 5, Figures S18 and S19). Based on the membrane disruption efficacy of Janus NPs, the phase diagram were divided into three regions. (i) In the region of high content of POPE but low content of LPS, both flat and curved membranes are disrupted by the Janus NP. (ii) At moderate LPS levels, only the curved membrane is disrupted, with a boundary at 60 mol% for ReLPS and 40 mol% for RaLPS, which indicates RaLPS's greater impact on interactions with curved membranes due to its bulkier conformation. (iii) When RaLPS and ReLPS exceeds 80 mol%, neither flat nor curved membranes are disrupted by the Janus NP, presumably because LPS at such high surface densities shields the lipid membrane from interaction with the NP. This diagram identifies a range of membrane compositions where Janus NPs can effectively disrupt curved but not flat membranes. Interestingly, this identified range is comparable to the range of LPS surface coverage observed in Gram-negative bacteria.[82-84]

This study challenges our current understanding of NP-bacteria interactions, by revealing a previously unseen phenomenon that NPs preferentially target and disrupt bacterial poles. We have previously shown that electrostatic attractions bring Janus NPs close to lipid membranes, while hydrophobic interactions drive lipid extraction and membrane disruption.[74, 92] However, in this study, by combining experimentation with CGMD modeling, we elucidate how cell wall curvature modulates the interaction between Janus NPs and the Gram-negative bacterium *E. coli*. Our findings reveal that as cationic Janus NPs are attracted to oppositely charged LPS on bacterial

membranes, curvature-induced conformational changes in LPS molecules expose the underlying lipid membrane, making the poles more susceptible to disruption by NPs driven by hydrophobic interactions. Our simulations yielded a comprehensive diagram that captures the interplay between LPS composition and NP-membrane interactions across a broad range of membrane compositions. This analysis highlights that curvature-induced targeting by NPs is most pronounced under physiologically relevant LPS densities, which underscores the real-world significance of our findings.

Importantly, this work challenges the typical assumption of a uniform bacterial cell wall in prior antibacterial NP studies. We demonstrate that high curvature creates weak spots on bacterial cell walls for antibacterial NPs, a concept previously overlooked. While our study emphasizes bacterial membrane curvature as a significant factor in Janus NP interactions, we acknowledge that other factors, such as membrane tension and lipid interactions in high-curvature regions, may also contribute. Previous studies show that bacteria can sense and regulate the tension of their outer membranes. In parallel, antibacterial nanoparticles – including those examined in our studies— have been found to alter the mechanical properties of bacterial membranes[74, 98] which can affect lipid and LPS packing and thus influence nanoparticle-membrane interactions, potentially creating a feedback loop of interactions. Given the emerging evidence of inherent cell wall heterogeneity in bacteria, understanding how its physical, mechanical, and chemical heterogeneities impact antibacterial nanoparticle action is critical for developing effective, targeted therapies.

ASSOCIATED CONTENT

Supporting Information.

The following files are available free of charge.

Experimental Methods, Computational Methods, Supplementary Figures including Figures S1-S19, Supplementary Tables including Tables S1-S4 (PDF)

Video S1: Time-lapse live-cell brightfield and fluorescence images showing Janus NPs binding to *E. coli* (MP4)

AUTHOR INFORMATION

Corresponding Author

*Yan Yu - Department of Chemistry, Indiana University, Bloomington, IN, 47405, United States; Email: yy33@indiana.edu

*Ying Li - Department of Mechanical Engineering, University of Wisconsin-Madison, Madison, WI, 53706, United States; Email: yli2562@wisc.edu

Author Contributions

†These authors contributed equally.

Funding Sources

The work was financially supported by the U.S. National Science Foundation under Awards CBET-2313754 (to Y.L.) and CBET- 2153891 (to Y.Y. and Y. L.). H. R. acknowledges receipt of a predoctoral fellowship from the Graduate Training Program in Quantitative and Chemical Biology at Indiana University (T32 GM131994). Support for this research was also provided by the University of Wisconsin–Madison, Office of the Vice Chancellor for Research and Graduate Education with funding from the Wisconsin Alumni Research Foundation.

Notes

The authors declare no competing financial interest.

ACKNOWLEDGMENT

We thank Prof. J. P. Gerdt at Indiana University for providing E. coli culture used in this study, Dr. Yi Yi and Dr. Jun Chen at IUB Nanoscale Characterization Facility for assistance with instrument use. The research was performed using computational resources sponsored by the Department of Energy's Office of Energy Efficiency and Renewable Energy and located at the National Renewable Energy Laboratory (Eagle Computing System).

REFERENCES

1. Tang, K. W. K.; Millar, B. C.; Moore, J. E., Antimicrobial Resistance (AMR). *Br J Biomed Sci* **2023,** *80*, 11387.

2. Gupta, A.; Mumtaz, S.; Li, C. H.; Hussain, I.; Rotello, V. M., Combatting antibiotic-resistant bacteria using nanomaterials. *Chem Soc Rev* **2019,** *48* (2), 415-427.

3. Huo, S.; Jiang, Y.; Gupta, A.; Jiang, Z.; Landis, R. F.; Hou, S.; Liang, X. J.; Rotello, V. M., Fully Zwitterionic Nanoparticle Antimicrobial Agents through Tuning of Core Size and Ligand Structure. *ACS Nano* **2016,** *10* (9), 8732-7.

4. Makabenta, J. M. V.; Nabawy, A.; Li, C. H.; Schmidt-Malan, S.; Patel, R.; Rotello, V. M., Nanomaterial-based therapeutics for antibiotic-resistant bacterial infections. *Nat Rev Microbiol* **2021,** *19* (1), 23-36.

5. Gao, W.; Zhang, L., Nanomaterials arising amid antibiotic resistance. *Nat Rev Microbiol* **2021,** *19* (1), 5-6.

6. Ndayishimiye, J.; Kumeria, T.; Popat, A.; Falconer, J. R.; Blaskovich, M. A. T., Nanomaterials: The New Antimicrobial Magic Bullet. *ACS Infect Dis* **2022,** *8* (4), 693-712.

7. Radovic-Moreno, A. F.; Lu, T. K.; Puscasu, V. A.; Yoon, C. J.; Langer, R.; Farokhzad, O. C., Surface Charge-Switching Polymeric Nanoparticles for Bacterial Cell Wall-Targeted Delivery of Antibiotics. *ACS Nano* **2012,** *6* (5), 4279-4287.

8. Pokhrel, L. R.; Jacobs, Z. L.; Dikin, D.; Akula, S. M., Five nanometer size highly positive silver nanoparticles are bactericidal targeting cell wall and adherent fimbriae expression. *Sci Rep* **2022,** *12* (1), 6729.

9. Gunawan, C.; Faiz, M. B.; Mann, R.; Ting, S. R. S.; Sotiriou, G. A.; Marquis, C. P.; Amal, R., Nanosilver Targets the Bacterial Cell Envelope: The Link with Generation of Reactive Oxygen Radicals. *ACS Appl Mater Interfaces* **2020,** *12* (5), 5557-5568.

10. Lemire, J. A.; Harrison, J. J.; Turner, R. J., Antimicrobial activity of metals: mechanisms, molecular targets and applications. *Nat Rev Microbiol* **2013,** *11* (6), 371-84.

11. Mammari, N.; Lamouroux, E.; Boudier, A.; Duval, R. E., Current Knowledge on the Oxidative-Stress-Mediated Antimicrobial Properties of Metal-Based Nanoparticles. *Microorganisms* **2022,** *10* (2).

12. Guerrero Correa, M.; Martinez, F. B.; Vidal, C. P.; Streitt, C.; Escrig, J.; de Dicastillo, C. L., Antimicrobial metal-based nanoparticles: a review on their synthesis, types and antimicrobial action. *Beilstein J Nanotechnol* **2020,** *11*, 1450-1469.

13. Okkeh, M.; Bloise, N.; Restivo, E.; De Vita, L.; Pallavicini, P.; Visai, L., Gold Nanoparticles: Can They Be the Next Magic Bullet for Multidrug-Resistant Bacteria? *Nanomaterials (Basel)* **2021,** *11* (2).

14. Prasad, K.; Lekshmi, G. S.; Ostrikov, K.; Lussini, V.; Blinco, J.; Mohandas, M.; Vasilev, K.; Bottle, S.; Bazaka, K.; Ostrikov, K., Synergic bactericidal effects of reduced graphene oxide and silver nanoparticles against Gram-positive and Gram-negative bacteria. *Sci Rep* **2017,** *7* (1), 1591.

15. Nederberg, F.; Zhang, Y.; Tan, J. P.; Xu, K.; Wang, H.; Yang, C.; Gao, S.; Guo, X. D.; Fukushima, K.; Li, L.; Hedrick, J. L.; Yang, Y. Y., Biodegradable nanostructures with selective lysis of microbial membranes. *Nat Chem* **2011,** *3* (5), 409-14.

16. Ramamurthi, K. S.; Losick, R., Negative membrane curvature as a cue for subcellular localization of a bacterial protein. *Proceedings of the National Academy of Sciences* **2009,** *106* (32), 13541-13545.

17. Moghadam, B. Y.; Hou, W. C.; Corredor, C.; Westerhoff, P.; Posner, J. D., Role of nanoparticle surface functionality in the disruption of model cell membranes. *Langmuir* **2012,** *28* (47), 16318-26.

18. De Nicola, A.; Montis, C.; Donati, G.; Molinaro, A.; Silipo, A.; Balestri, A.; Berti, D.; Di Lorenzo, F.; Zhu, Y. L.; Milano, G., Bacterial lipids drive compartmentalization on the nanoscale. *Nanoscale* **2023,** *15* (20), 8988-8995.

19. Marin-Menendez, A.; Montis, C.; Diaz-Calvo, T.; Carta, D.; Hatzixanthis, K.; Morris, C. J.; McArthur, M.; Berti, D., Antimicrobial Nanoplexes meet Model Bacterial Membranes: the key role of Cardiolipin. *Sci Rep* **2017,** *7*, 41242.

20. Chen, K. L.; Bothun, G. D., Nanoparticles meet cell membranes: probing nonspecific interactions using model membranes. *Environ Sci Technol* **2014,** *48* (2), 873-80.

21. Chakraborty, A.; Kobzev, E.; Chan, J.; de Zoysa, G. H.; Sarojini, V.; Piggot, T. J.; Allison, J. R., Molecular Dynamics Simulation of the Interaction of Two Linear Battacin Analogs with Model Gram-Positive and Gram-Negative Bacterial Cell Membranes. *ACS Omega* **2021,** *6* (1), 388-400.

22. Jacobson, K. H.; Gunsolus, I. L.; Kuech, T. R.; Troiano, J. M.; Melby, E. S.; Lohse, S. E.; Hu, D.; Chrisler, W. B.; Murphy, C. J.; Orr, G.; Geiger, F. M.; Haynes, C. L.; Pedersen, J. A., Lipopolysaccharide Density and Structure Govern the Extent and Distance of Nanoparticle Interaction with Actual and Model Bacterial Outer Membranes. *Environ Sci Technol* **2015,** *49* (17), 10642-50.

23. Tu, Y.; Lv, M.; Xiu, P.; Huynh, T.; Zhang, M.; Castelli, M.; Liu, Z.; Huang, Q.; Fan, C.; Fang, H.; Zhou, R., Destructive extraction of phospholipids from Escherichia coli membranes by graphene nanosheets. *Nat Nanotechnol* **2013,** *8* (8), 594-601.

24. Fuster, M. G.; Montalban, M. G.; Carissimi, G.; Lima, B.; Feresin, G. E.; Cano, M.; Giner-Casares, J. J.; Lopez-Cascales, J. J.; Enriz, R. D.; Villora, G., Antibacterial Effect of Chitosan-Gold Nanoparticles and Computational Modeling of the Interaction between Chitosan and a Lipid Bilayer Model. *Nanomaterials (Basel)* **2020,** *10* (12).

25. Tsukanov, A. A.; Pervikov, A. V.; Lozhkomoev, A. S., Bimetallic Ag–Cu nanoparticles interaction with lipid and lipopolysaccharide membranes. *Computational Materials Science* **2020,** *173*.

26. Razavi, R.; Amiri, M.; Alshamsi, H. A.; Eslaminejad, T.; Salavati-Niasari, M., Green synthesis of Ag nanoparticles in oil-in-water nano-emulsion and evaluation of their antibacterial and cytotoxic properties as well as molecular docking. *Arabian Journal of Chemistry* **2021,** *14* (9).

27. Giulini, M.; Rigoli, M.; Mattiotti, G.; Menichetti, R.; Tarenzi, T.; Fiorentini, R.; Potestio, R., From System Modeling to System Analysis: The Impact of Resolution Level and Resolution Distribution in the Computer-Aided Investigation of Biomolecules. *Front Mol Biosci* **2021,** *8*, 676976.

28. Hsu, P. C.; Jefferies, D.; Khalid, S., Molecular Dynamics Simulations Predict the Pathways via Which Pristine Fullerenes Penetrate Bacterial Membranes. *J Phys Chem B* **2016,** *120* (43), 11170-11179.

29. Marrink, S. J.; Risselada, H. J.; Yefimov, S.; Tieleman, D. P.; de Vries, A. H., The MARTINI Force Field: Coarse Grained Model for Biomolecular Simulations. *The Journal of Physical Chemistry B* **2007,** *111* (27), 7812-7824.

30. Pal, I.; Bhattacharyya, D.; Kar, R. K.; Zarena, D.; Bhunia, A.; Atreya, H. S., A Peptide-Nanoparticle System with Improved Efficacy against Multidrug Resistant Bacteria. *Sci Rep* **2019,** *9* (1), 4485.

31. Dai, S.; Ye, R.; Huang, J.; Wang, B.; Xie, Z.; Ou, X.; Yu, N.; Huang, C.; Hua, Y.; Zhou, R.; Tian, B., Distinct lipid membrane interaction and uptake of differentially charged nanoplastics in bacteria. *J Nanobiotechnology* **2022,** *20* (1), 191.

32. Mathelie-Guinlet, M.; Asmar, A. T.; Collet, J. F.; Dufrene, Y. F., Lipoprotein Lpp regulates the mechanical properties of the E. coli cell envelope. *Nat Commun* **2020,** *11* (1), 1789.

33. Sun, J.; Rutherford, S. T.; Silhavy, T. J.; Huang, K. C., Physical properties of the bacterial outer membrane. *Nat Rev Microbiol* **2022,** *20* (4), 236-248.

34. Mukhopadhyay, R.; Huang, K. C.; Wingreen, N. S., Lipid localization in bacterial cells through curvature-mediated microphase separation. *Biophys J* **2008,** *95* (3), 1034-49.

35. Barák, I.; Muchová, K. The Role of Lipid Domains in Bacterial Cell Processes *International Journal of Molecular Sciences* [Online], 2013, p. 4050-4065.

36. Beltran-Heredia, E.; Tsai, F. C.; Salinas-Almaguer, S.; Cao, F. J.; Bassereau, P.; Monroy, F., Membrane curvature induces cardiolipin sorting. *Commun Biol* **2019,** *2*, 225.

37. Laloux, G.; Jacobs-Wagner, C., How do bacteria localize proteins to the cell pole? *J Cell Sci* **2014,** *127* (Pt 1), 11-9.

38. Renner, L. D.; Weibel, D. B., Cardiolipin microdomains localize to negatively curved regions of Escherichia coli membranes. *Proc Natl Acad Sci U S A* **2011,** *108* (15), 6264-9.

39. Huang, K. C.; Mukhopadhyay, R.; Wingreen, N. S., A curvature-mediated mechanism for localization of lipids to bacterial poles. *PLoS Comput Biol* **2006,** *2* (11), e151.

40. Mileykovskaya, E.; Dowhan, W., Visualization of Phospholipid Domains inEscherichia coli by Using the Cardiolipin-Specific Fluorescent Dye 10-N-Nonyl Acridine Orange. *Journal of Bacteriology* **2000,** *182* (4), 1172-1175.

41. Koldso, H.; Shorthouse, D.; Helie, J.; Sansom, M. S., Lipid clustering correlates with membrane curvature as revealed by molecular simulations of complex lipid bilayers. *PLoS Comput Biol* **2014,** *10* (10), e1003911.

42. Risselada, H. J.; Marrink, S. J., Curvature effects on lipid packing and dynamics in liposomes revealed by coarse grained molecular dynamics simulations. *Physical Chemistry Chemical Physics* **2009,** *11* (12), 2056-2067.

43. Nishizawa, M.; Nishizawa, K., Curvature-driven lipid sorting: coarse-grained dynamics simulations of a membrane mimicking a hemifusion intermediate. *Journal of Biophysical Chemistry* **2010,** *01* (02), 86-95.

44. Barragan Vidal, I. A.; Rosetti, C. M.; Pastorino, C.; Muller, M., Measuring the composition-curvature coupling in binary lipid membranes by computer simulations. *J Chem Phys* **2014,** *141* (19), 194902.

45. Elias-Wolff, F.; Linden, M.; Lyubartsev, A. P.; Brandt, E. G., Curvature sensing by cardiolipin in simulated buckled membranes. *Soft Matter* **2019,** *15* (4), 792-802.

46. Golla, V. K.; Boyd, K. J.; May, E. R., Curvature sensing lipid dynamics in a mitochondrial inner membrane model. *Commun Biol* **2024,** *7* (1), 29.

47. Cino, E. A.; Tieleman, D. P., Curvature-based sorting of eight lipid types in asymmetric buckled plasma membrane models. *Biophys J* **2022,** *121* (11), 2060-2068.

48. Yesylevskyy, S.; Martinez-Seara, H.; Jungwirth, P., Curvature Matters: Modeling Calcium Binding to Neutral and Anionic Phospholipid Bilayers. *J Phys Chem B* **2023,** *127* (20), 4523-4531.

49. Yesylevskyy, S.; Rivel, T.; Ramseyer, C., Curvature increases permeability of the plasma membrane for ions, water and the anti-cancer drugs cisplatin and gemcitabine. *Sci Rep* **2019,** *9* (1), 17214.

50. van Hilten, N.; Methorst, J.; Verwei, N.; Risselada, H. J., Physics-based generative model of curvature sensing peptides; distinguishing sensors from binders. *Science Advances* **2023,** *9* (11), eade8839.

51. Kasson, P. M.; Pande, V. S., Control of membrane fusion mechanism by lipid composition: predictions from ensemble molecular dynamics. *PLoS Comput Biol* **2007,** *3* (11), e220.

52. Woodward, X.; Javanainen, M.; Fábián, B.; Kelly, C. V., Nanoscale membrane curvature sorts lipid phases and alters lipid diffusion. *Biophysical Journal* **2023,** *122* (11), 2203-2215.

53. Klaus, C. J.; Raghunathan, K.; DiBenedetto, E.; Kenworthy, A. K., Analysis of diffusion in curved surfaces and its application to tubular membranes. *Mol Biol Cell* **2016,** *27* (24), 3937-3946.

54. Epand, R. M.; Epand, R. F., Lipid domains in bacterial membranes and the action of antimicrobial agents. *Biochim Biophys Acta* **2009,** *1788* (1), 289-94.

55. Rosa Eugenia, R.; Carolina Romo, G. l.; Rafael Coria, J. n.; Maribel Ortiz, H.; Alejandra Aquino, A., Mechanisms of O-Antigen Structural Variation of Bacterial

Lipopolysaccharide (LPS). In *The Complex World of Polysaccharides*, Desiree Nedra, K., Ed. IntechOpen: Rijeka, 2012; p Ch. 3.

56. Sohlenkamp, C.; Geiger, O., Bacterial membrane lipids: diversity in structures and pathways. *FEMS Microbiol Rev* **2016,** *40* (1), 133-59.

57. Lee, T.-H.; Hofferek, V.; Separovic, F.; Reid, G. E.; Aguilar, M.-I., The role of bacterial lipid diversity and membrane properties in modulating antimicrobial peptide activity and drug resistance. *Current Opinion in Chemical Biology* **2019,** *52*, 85-92.

58. Zhulina, E. B.; Borisov, O. V., Polyelectrolytes Grafted to Curved Surfaces. *Macromolecules* **1996,** *29* (7), 2618-2626.

59. Gonzalez Solveyra, E.; Thompson, D. H.; Szleifer, I., Proteins Adsorbing onto Surface-Modified Nanoparticles: Effect of Surface Curvature, pH, and the Interplay of Polymers and Proteins Acid-Base Equilibrium. *Polymers (Basel)* **2022,** *14* (4).

60. Liu, H.; Zhu, Y. L.; Zhang, J.; Lu, Z. Y.; Sun, Z. Y., Influence of Grafting Surface Curvature on Chain Polydispersity and Molecular Weight in Concave Surface-Initiated Polymerization. *ACS Macro Lett* **2012,** *1* (11), 1249-1253.

61. Laktionov, M. Y.; Zhulina, E. B.; Richter, R. P.; Borisov, O. V., Polymer Brush in a Nanopore: Effects of Solvent Strength and Macromolecular Architecture Studied by Self-Consistent Field and Scaling Theory. *Polymers (Basel)* **2021,** *13* (22).

62. Lin, J.; Zhang, H.; Morovati, V.; Dargazany, R., PEGylation on mixed monolayer gold nanoparticles: Effect of grafting density, chain length, and surface curvature. *J Colloid Interface Sci* **2017,** *504*, 325-333.

63. Xue, Y.-H.; Zhu, Y.-L.; Quan, W.; Qu, F.-H.; Han, C.; Fan, J.-T.; Liu, H., Polymer-grafted nanoparticles prepared by surface-initiated polymerization: the characterization of

polymer chain conformation, grafting density and polydispersity correlated to the grafting surface curvature. *Physical Chemistry Chemical Physics* **2013,** *15* (37), 15356-15364.

64. Conrad, J. C.; Robertson, M. L., Shaping the Structure and Response of Surface-Grafted Polymer Brushes via the Molecular Weight Distribution. *JACS Au* **2023,** *3* (2), 333-343.

65. Oyerokun, F. T.; Vaia, R. A., Distribution in the Grafting Density of End-Functionalized Polymer Chains Adsorbed onto Nanoparticle Surfaces. *Macromolecules* **2012,** *45* (18), 7649-7659.

66. Moussavi, A.; Pal, S.; Wu, Z.; Keten, S., Characterizing the shear response of polymer-grafted nanoparticles. *J Chem Phys* **2024,** *160* (13).

67. Dimitrov, D. I.; Milchev, A.; Binder, K., Polymer brushes in cylindrical pores: simulation versus scaling theory. *J Chem Phys* **2006,** *125* (3), 34905.

68. Milchev, A.; Petkov, P., Concave polymer brushes inwardly grafted in spherical cavities. *The Journal of Chemical Physics* **2023,** *158* (9).

69. Polanowski, P.; Jeszka, J. K.; Matyjaszewski, K., Polymer brushes in pores by ATRP: Monte Carlo simulations. *Polymer* **2020,** *211*.

70. Chen, G.; Dormidontova, E., PEO-Grafted Gold Nanopore: Grafting Density, Chain Length, and Curvature Effects. *Macromolecules* **2022,** *55* (12), 5222-5232.

71. Lee, K.; Yu, Y., Lipid Bilayer Disruption by Amphiphilic Janus Nanoparticles: The Role of Janus Balance. *Langmuir* **2018,** *34* (41), 12387-12393.

72. Lee, K.; Zhang, L.; Yi, Y.; Wang, X.; Yu, Y., Rupture of Lipid Membranes Induced by Amphiphilic Janus Nanoparticles. *ACS Nano* **2018,** *12* (4), 3646-3657.

73. Wiemann, J. T.; Shen, Z.; Ye, H.; Li, Y.; Yu, Y., Membrane poration, wrinkling, and compression: deformations of lipid vesicles induced by amphiphilic Janus nanoparticles. *Nanoscale* **2020,** *12* (39), 20326-20336.

74. Wiemann, J. T.; Nguyen, D.; Bhattacharyya, S.; Li, Y.; Yu, Y., Antibacterial Activity of Amphiphilic Janus Nanoparticles Enhanced by Polycationic Ligands. *ACS Applied Nano Materials* **2023,** *6* (21), 20398-20409.

75. Renner, L. D.; Weibel, D. B., Cardiolipin microdomains localize to negatively curved regions of Escherichia coli membranes. *Proceedings of the National Academy of Sciences* **2011,** *108* (15), 6264-6269.

76. Phanphak, S.; Georgiades, P.; Li, R.; King, J.; Roberts, I. S.; Waigh, T. A., Super-Resolution Fluorescence Microscopy Study of the Production of K1 Capsules by Escherichia coli: Evidence for the Differential Distribution of the Capsule at the Poles and the Equator of the Cell. *Langmuir* **2019,** *35* (16), 5635-5646.

77. Zhou, T.; Qi, H.; Han, L.; Barbash, D.; Li, C. Y., Towards controlled polymer brushes via a self-assembly-assisted-grafting-to approach. *Nature Communications* **2016,** *7* (1), 11119.

78. Pavón, C.; Benetti, E. M.; Lorandi, F., Polymer Brushes on Nanoparticles for Controlling the Interaction with Protein-Rich Physiological Media. *Langmuir* **2024**, 40 (23), 11843–11857.

79. Binder, K.; Milchev, A., Polymer brushes on flat and curved surfaces: How computer simulations can help to test theories and to interpret experiments. *Journal of Polymer Science Part B: Polymer Physics* **2012,** *50* (22), 1515-1555.

80. Hsu, P.-C.; Bruininks, B. M. H.; Jefferies, D.; Cesar Telles de Souza, P.; Lee, J.; Patel, D. S.; Marrink, S. J.; Qi, Y.; Khalid, S.; Im, W., CHARMM-GUI Martini Maker for modeling

and simulation of complex bacterial membranes with lipopolysaccharides. *Journal of Computational Chemistry* **2017,** *38* (27), 2354-2363.

81. Murzyn, K.; Rog, T.; Pasenkiewicz-Gierula, M., Phosphatidylethanolamine-phosphatidylglycerol bilayer as a model of the inner bacterial membrane. *Biophys J* **2005,** *88* (2), 1091-103.

82. Saini, G.; Wood, B. D., Preparation and characterization of lipopolysaccharide (LPS) monolayers for investigating their role in bacterial adhesion. *Materials Today: Proceedings* **2020,** *29*, 895-900.

83. Casillo, A.; Parrilli, E.; Tutino, M. L.; Corsaro, M. M., The outer membrane glycolipids of bacteria from cold environments: isolation, characterization, and biological activity. *FEMS Microbiology Ecology* **2019,** *95* (7), fiz094, pp 1-14.

84. Perrella, A.; Carannante, N.; Capoluongo, N.; Mascolo, A.; Capuano, A., Endotoxin: Structure Source and Effects. In *Endotoxin Induced-Shock: a Multidisciplinary Approach in Critical Care*, De Rosa, S.; Villa, G., Eds. Springer International Publishing: Cham, 2023; pp 1-11.

85. Dai, S.; Ye, R.; Huang, J.; Wang, B.; Xie, Z.; Ou, X.; Yu, N.; Huang, C.; Hua, Y.; Zhou, R.; Tian, B., Distinct lipid membrane interaction and uptake of differentially charged nanoplastics in bacteria. *Journal of Nanobiotechnology* **2022,** *20* (1), 191.

86. Tu, Y.; Lv, M.; Xiu, P.; Huynh, T.; Zhang, M.; Castelli, M.; Liu, Z.; Huang, Q.; Fan, C.; Fang, H.; Zhou, R., Destructive extraction of phospholipids from Escherichia coli membranes by graphene nanosheets. *Nature Nanotechnology* **2013,** *8* (8), 594-601.

87. Fuster, M. G.; Montalbán, M. G.; Carissimi, G.; Lima, B.; Feresin, G. E.; Cano, M.; Giner-Casares, J. J.; López-Cascales, J. J.; Enriz, R. D.; Víllora, G. Antibacterial Effect of

Chitosan–Gold Nanoparticles and Computational Modeling of the Interaction between Chitosan and a Lipid Bilayer Model. *Nanomaterials*, **2020**, 10(12), 2340.

88. Pal, I.; Bhattacharyya, D.; Kar, R. K.; Zarena, D.; Bhunia, A.; Atreya, H. S., A Peptide-Nanoparticle System with Improved Efficacy against Multidrug Resistant Bacteria. *Scientific Reports* **2019,** *9* (1), 4485.

89. Ou, L.; Chen, H.; Yuan, B.; Yang, K., Membrane-Specific Binding of 4 nm Lipid Nanoparticles Mediated by an Entropy-Driven Interaction Mechanism. *ACS Nano* **2022,** *16* (11), 18090-18100.

90. Foreman-Ortiz, I. U.; Liang, D.; Laudadio, E. D.; Calderin, J. D.; Wu, M.; Keshri, P.; Zhang, X.; Schwartz, M. P.; Hamers, R. J.; Rotello, V. M.; Murphy, C. J.; Cui, Q.; Pedersen, J. A., Anionic nanoparticle-induced perturbation to phospholipid membranes affects ion channel function. *Proceedings of the National Academy of Sciences* **2020,** *117* (45), 27854-27861.

91. Lin, J.; Zhang, H.; Morovati, V.; Dargazany, R., PEGylation on mixed monolayer gold nanoparticles: Effect of grafting density, chain length, and surface curvature. *Journal of Colloid and Interface Science* **2017,** *504*, 325-333.

92. Nguyen, D.; Wu, J.; Corrigan, P.; Li, Y., Computational investigation on lipid bilayer disruption induced by amphiphilic Janus nanoparticles: combined effect of Janus balance and charged lipid concentration. *Nanoscale* **2023,** *15* (39), 16112-16130.

93. Zhou, J.; Cai, Y.; Liu, Y.; An, H.; Deng, K.; Ashraf, M. A.; Zou, L.; Wang, J., Breaking down the cell wall: Still an attractive antibacterial strategy. *Front Microbiol* **2022,** *13*, 952633.

94. Odjadjare, E. C.; Olaniran, A. O. Prevalence of Antimicrobial Resistant and Virulent Salmonella spp. in Treated Effluent and Receiving Aquatic Milieu of Wastewater Treatment

Plants in Durban, South Africa *International Journal of Environmental Research and Public Health* [Online], 2015, p. 9692-9713.

95. Epand, R. M.; Epand, R. F., Lipid domains in bacterial membranes and the action of antimicrobial agents. *Biochimica et Biophysica Acta (BBA) - Biomembranes* **2009,** *1788* (1), 289-294.

96. Epand, R. M.; Walker, C.; Epand, R. F.; Magarvey, N. A., Molecular mechanisms of membrane targeting antibiotics. *Biochimica et Biophysica Acta (BBA) - Biomembranes* **2016,** *1858* (5), 980-987.

97. Nathwani, D.; Raman, G.; Sulham, K.; Gavaghan, M.; Menon, V., Clinical and economic consequences of hospital-acquired resistant and multidrug-resistant Pseudomonas aeruginosa infections: a systematic review and meta-analysis. *Antimicrobial Resistance and Infection Control* **2014,** *3* (1), 32.

98. Linklater, D. P.; Baulin, V. A.; Le Guével, X.; Fleury, J.-B.; Hanssen, E.; Nguyen, T. H. P.; Juodkazis, S.; Bryant, G.; Crawford, R. J.; Stoodley, P.; Ivanova, E. P., Antibacterial Action of Nanoparticles by Lethal Stretching of Bacterial Cell Membranes. *Adv. Mater.* **2020,** *32* (52), 2005679.